Energy Science & Engineering

ORIGINAL ARTICLE

An experimental and numerical investigation of the effects of the diaphragm pressure ratio and its position on a heated shock tube performance

Yousif Badri | Aboubaker Elbashir | Ahmad Saker | Samer F. Ahmed

Department of Mechanical and Industrial Engineering, Qatar University, Doha, Qatar

Correspondence
Samer F. Ahmed, Department of Mechanical and Industrial Engineering, Qatar University, PO Box 2713, Doha, Qatar.
Email: sahmed@qu.edu.qa

Abstract

The main purpose of this work was to investigate the performance of heated shock tube (ST) with different pressure ratios and diaphragm positions numerically and experimentally. The numerical model was developed to simulate the fluid flow inside a shock tube test facility located at Qatar University. The shock tube was a cast-iron hollow tube with 6 m length, 50 mm internal diameter and 10 mm thickness. ST driver and driven sections were filled with helium–argon mixture and air. The driven section was heated up to 150°C using coils. At the middle of the ST, the diaphragm was made of aluminium sheet (0.5 mm) layers. Five different pressure ratios were implemented during the experiment, and performance evaluation depended on the strength of the incident shock Mach number. The inviscid numerical model solver used transient two-dimensional time-accurate Navier–Stokes CFD. The model introduced a parametric study regarding three different diaphragm positions (1m, 2m and 3m) and five pressure ratios (6–10) for each position. In addition to yielding the incident and reflected wave Mach number, reflected wave temperature was also considered a shock tube performance indicator. The incident Mach numbers for the diaphragm middle position from the experiment were compared against those conducted from the model, and good matching was observed. The parametric study results showed that at high-pressure ratios, diaphragm Positions 1 and 3 could generate a 7.4% increase in shock wave Mach number compared with the diaphragm position-2 model. Moreover, the diaphragm position-3 model tends to have a 2% increase in the temperature behind the reflected shock wave compared with the other two positions.

KEYWORDS
diaphragm position and pressure ratio, incident Mach number8, inviscid model, reflected wave, shock tube

1 | INTRODUCTION

A shock tube (ST) is a well-established facility where an unsteady flow gas dynamic one-dimensional problem can be solved by producing a shock wave in a controllable manner. Shock tubes have been used to serve several applications such as aerodynamic study, high-temperature chemical kinetic applications, material interaction to the shock waves, blast waves, industrial implementations and recently biomedical applications.[1-4] A shock tube is also used extensively in simulating the chemical kinetics of combustion for different fuels. A variety of recent studies were conducted involved using shock tubes along with high-density fuel/air mixtures to obtain combustion features of conventional and alternative fuels at conditions relevant to those used in internal combustion engines and gas turbine machines.[5-8] Ignition delay time (IDT), particularly in internal combustion engines, is a vital combustion characteristic that directly affects engine efficiency and exhaust emissions.[9-13] This property in ICE can be defined as the time required to detect heat release once the air–fuel mixture reaches the self-ignition (autoignition) temperature and pressure or the time interval between the start of ignition (raising injector needle) and the beginning of combustion.[14] The total delay period is due to a combination of physical and chemical delays. Physical delay is due to fuel atomization, evaporation and mixing with air.

As a result, fuel properties and the mixture pressure, temperature and velocity will influence the ignition delay. Thus, the fuel injection system, combustion chamber and engine operating conditions are the main factors of controlling the above parameters. Due to the shock tube conditions, which simulate ICE combustion, IDTs of different fuel types can be measured using a shock tube. It should be mentioned that the shock tube can only measure the chemical delay of pre-combustion reactions for a homogeneous air–fuel mixture. IDT can be investigated using several facilities such as a ST, rapid compression machine (RCM) and constant volume bomb (CVB). A shock wave is designed to permeate through the air–fuel mixture using a driver inert gas, leading to ignition of an air-fuel mixture under certain initial pressure, temperature and equivalence ratio conditions. In conventional ST, a high-pressure inert gas in the driver section ruptures a diaphragm that separates ST's two segments (driver and driven).
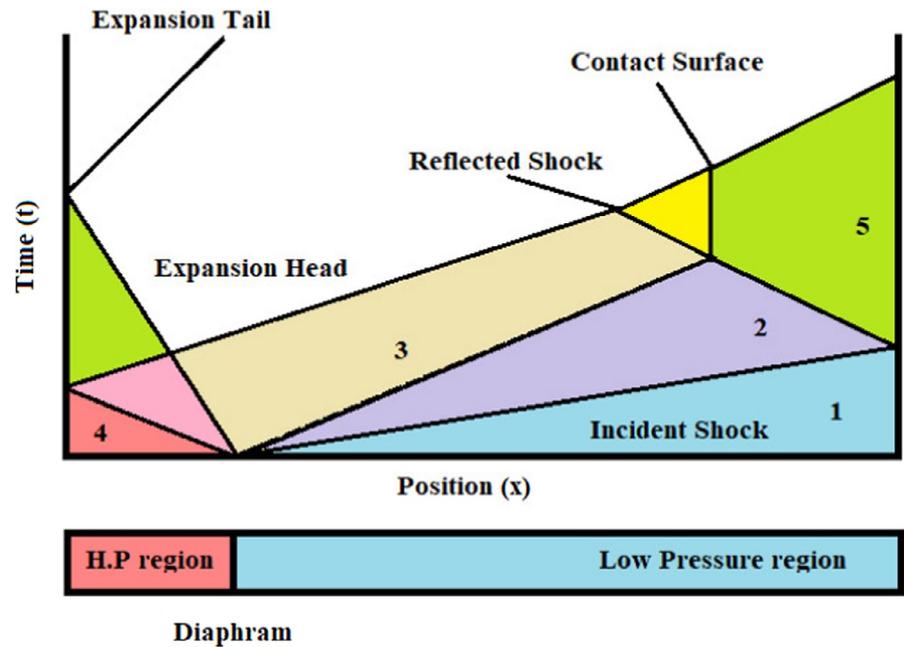
Numerous studies about different ST designs were developed to obtain accurate IDT measurements. For example, the diaphragm less ST idea was introduced by Tranter and Giri[15] and Nagaraja et al.[16] They replaced the conventional metallic diaphragm with a fast-acting piston valve. It was found that this concept improves the repeatability of the results, produces a reliable generation of shock waves and enhances the signal/noise ratio and mass peak efficiency. However, this technique cannot be used with a traditional shock tube. Another improvement in ST design used in IDT investigations is the aerosol ST.[17-21] The advantage of this design is that the standard ST is more appropriate for studying gaseous fuels, however, it is difficult to obtain a homogenous mixture for liquid fuels such as diesel, gasoline and jet fuels (low vapour pressure fuels). Furthermore, the non-homogeneous mix can lead to an in-spatial spread of the aerosol and non-uniformity, restricting measurement precision, incident determination and reflected shock wave conditions. An ideal flow schematic of the shock tube facility is shown in Figure 1.

Usually, the diaphragm is assumed to rapture at $t = 0$, and before the rapture, only two regions exist, 4 and 1, which indicates the high and low-pressure regions, respectively. After the rapture, a compression wave is developed in the driven section (low pressure), generating region (2) behind it. In addition to the compression wave, an expansion wave is formed at the driver section lowering its high-pressure value and forming a new region (State 3). Next, the compression wave is reflected from the high temperature and pressure of the driver end-wall, creating a region (5). Finally, the expansion wave is also reflected when it reaches the driver's left end and significantly increases pressure and temperature. The region behind the reflected expansion wave is illustrated as Stage 6 in Figure 1. Eventually, all the regions will reach a steady-state condition with constant pressure and temperature throughout the inner volume of the ST.

Many scholars investigated experimentally and numerically the parameters that affect the performance of shock tubes. Luan et al.[22] investigated the flow numerically inside a shock tube with a small nozzle at the end of the driven section. They use two models: pressure-based and density-based models. Both numerical simulations were evaluated with an analytical solution of Sod's problem.[23] The comparison showed that, for high temperatures, a density-based second-order ROE is suitable for accurately predicting the flow properties inside the shock tube. Moradi et al.[24] investigated experimentally and numerically the aerothermodynamic properties of a shock wave at the walls of a shock tube. Experimentally, they built a shock tube facility with a driver section connected to a pressurized tank, and the drive section is open to the atmosphere. The diaphragm was made of aluminium foil having thicknesses of 50 and 80 μm destructed in 2.7 and 4.8 bar, respectively. They stimulate the flow inside the shock tube as a laminar regime using CFD. They used the pressure-based model with the simple mode for pressure–velocity coupling in the second order for the model solver. Two pressure ratios were investigated regarding the two diaphragm destruction pressures. The numerical model

pressure distributions and velocity profiles for the two cases clarify the velocity increase as the driver pressure increases.

In another study, Jayakumar[25] conducted a numerical model to test the effect of increasing the pressure ratio in a shock tube. The main objective was to compare the performance of two model gases, carbon dioxide and air, as working fluids inside the driver section of the shock tube. Their numerical study used fluent density-based in Ansys CFD to model the flow of gases inside the shock tube as inviscid flow. For different diaphragm pressure ratios, the shock Mach number, pressure and temperature behind the incident and reflected waves were obtained for the two gases models. The results showed that using carbon dioxide as a working fluid resulted in a higher Mach number when increasing the pressure ratio than when using air. Moreover, carbon dioxide generated a low temperature behind the incident and reflected shock waves compared with air.[26,27]

A recent study delivered by Ananthu and Asok Kumar[28] investigated the effect of the diaphragm pressure ratio on shock wave Mach number and temperature. The parametric study used three driver-driven gas models: helium (He)–CO_2, He–He and CO_2–CO_2. An inviscid-transient model was adopted for the study using CFD solver in Ansys FLUENT 18. The two-dimensional numerical model results were validated with a 1-dimensional ideal theory of Rankine–Hugoniot relations. The results showed that the He-CO_2 mixture gives the highest Mach number compared with the other working fluids for the same pressure ratios. The Mach number increased by about 20.4% for lower pressure ratios, while high-pressure ratios developed a 33% hike in Mach number for

the different gas models. In addition, using He with the same gas model gave the highest temperature behind the reflected shock wave compared with other gases models used in the study.[28] The literature showed a high tendency to use the 2D inviscid-transient CFD model to simulate the fluid flow inside the shock tube. It also showed that several studies investigated the shock tube performance when changing parameters such as pressure ratios and diaphragm positions. However, none studied these parameters with a heated driven section and validated the model with experimental results. Therefore, a numerical and experimental parametric study was conducted for a heated shock tube in this paper. The contribution of this paper is mainly to predict the effect of changing diaphragm positions and pressure ratios on the wave propagation along the heated driven section. It should be mentioned that the flow discontinuity characteristics of yield in Mach and the wave temperature have been considered to be the leading indicators of shock tube performance. The accuracy range of the numerical model was assessed with an experimental test that included all the pressure ratios with each diaphragm position.

2 | EXPERIMENTAL METHODS

The experimental study was conducted by using a standard shock tube test facility, as shown in Figure 2. In brief, it consists of a long tube with a 6 m length of 120 times the tube diameter (50 mm), as stated by Bradley and Emrich.[29] The length-internal diameter ratio was determined to avoid catching up with the reflected rarefaction wave with the incident shock wave before the incident

shock is generated inside the tube.[29] The tube is divided into two parts: driver section (3m) and driven section or test section (3m) (Figure 3). A thin aluminium diaphragm of 0.5 mm separates the two segments. The diaphragm thickness was chosen based on the rupture pressure of the diaphragm. The diaphragm breaking mechanism required 0.9 bar pressure per one aluminium layer to cause the foil rapture. The driver gases (He and Ar) were obtained from two pressurized cylinders using mass flow controllers (MFC) with a helium percentage of 5%–20% of argon in the mixture inside the driver section. A pressure gauge was mounted at the tube inlet to adjust the required quantities of the driver gases at the driver section. Two pressure transducers (PXM01MD0)[30] were screw-mounted to the tube wall; the first one is 1 m apart from the tube end-wall with an uncertainty of 0.1%. The second transducer was mounted 10 cm apart from the diaphragm location with the same uncertainty.

On the contrary, a pressure relief valve was fixed 20 cm apart from the diaphragm in the heated section to evacuate the tube from gases, as shown in Figure 3. Electric heaters of 900 W capacity were used to heat the air to maintain a temperature of 150°C. The temperature measurements of the heated section were carried out using a type k thermocouple connected to the data acquisition system (DAQ) with a measurement accuracy of 0.1%. A

thermal ceramic fibre insulator was used to isolate the driven part (heated section) with thermal conductivity of about 0.0346 W/m·K.

The experiment started by feeding the driver section with the working fluid (10% Ar, 90% He). A pressure gauge is attached to the driver left end-wall to measure pressure. A valve is located 2m away from the left driver section end-wall to store the gas in the driver section until it reaches the desired pressure value. The pressurized gas in the driver section was released when the valve was opened to cause diaphragm rapture.

After releasing the stored gases in the driver section, the high-pressure fluid flowed and raptured the middle diaphragm. The shock wave was propagating in the driven part with a high velocity, changing the local pressure of the sensor to a specific value. The main aim of this experiment was to calculate the wave velocity at the instant of rapture before the wave reflection took place. The shock wave velocity was detected by knowing the time required for the wave to pass through the two sensors. The two pressure sensors recorded the increase in pressure at the oscilloscope, and the interval between the two pressure peaks was obtained. The required wave velocity can be found by considering the distance separating the two sensors then dividing it by the wave travelling time. The previous experimental procedure was repeated many times at different
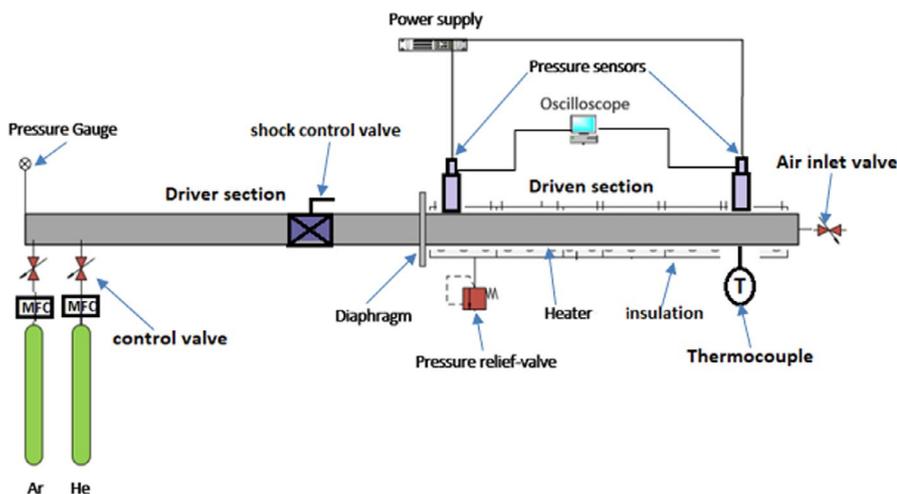
pressure ratios of the parametric study. Although one position was considered in the experimental setup (diaphragm at 3m), it was necessary to validate the numerical model. The shock tube measurements have several obstacles, including non-ideal effects, restricted test time availability and a lack of agreement on defining measurement errors. For the new shock tube to be evaluated in terms of performance, it must calculate the error percentage of all of the related measurements. The distance and the time it takes for the shock wave to travel between side-wall transducers have a role in shock velocity measurement.[31] Therefore, the accuracy of both of these measurements is critical. The size and location of the transducer holes and the geometry of the driven section are potential causes of inaccuracy for distance measurement.

Furthermore, the electrical equipment used for time measurement (counters, wires and pressure transducers) has the same characteristics. The theory of uncertainty propagation is used to calculate the overall uncertainty in shock velocity measurements. For a shock travelling at (Mach number between 1.2 and 1.6) between transducers 250 cm apart, this interval corresponds to a standard uncertainty of 0.1% of the measured time. The estimated uncertainty on the distance between the ends of successive pairs of holes in the tube wall is 0.15 mm.

3 | NUMERICAL MODEL

The flow of Argon and Helium mixture from the driver section into the driven section with diaphragm rapture was simulated using CFD solver Ansys Fluent 17. A two-dimensional inviscid density-based time-accurate model was developed to conduct the parametric study. The inviscid model discarded the viscosity effect and reduced the Navier–Stokes equation to the Euler equation.

3.1 | Governing equations

Since the viscous effect is negligible for a flow with a high Reynold number, the flow inside the tube was assumed to be inviscid. Non-viscous flow consideration reduces the Navier–stoke equation to the Euler equation. Euler equation is a non-linear hyperbolic differential equation. Therefore, the Euler equation can only be seen as the Navier–Stokes equation with zero viscosity and zero thermal conductivity. The Euler equations used for the present numerical model are as follows:

$$\frac{\partial U}{\partial t} + \frac{\partial E}{\partial x} + \frac{\partial F}{\partial y} = 0 \tag{1}$$

where U represents the conserved variable of the Euler equation in two-dimension Cartesian coordinates. The E and F variables, along with U variable definitions, are given below in Equation (2)

$$U = \begin{bmatrix} \rho \\ \rho u \\ \rho v \\ \varepsilon \end{bmatrix}, E = \begin{bmatrix} \rho u \\ \rho u^2 + p \\ \rho uv \\ \varepsilon \end{bmatrix}, F = \begin{bmatrix} \rho v \\ \rho uv \\ \rho v^2 + p \\ v(\varepsilon + p) \end{bmatrix} \tag{2}$$

Since the energy equation was activated in the CFD model, the below equations are included in the numerical model.

$$\varepsilon = \frac{1}{\gamma - 1} \left(\frac{P}{\rho} \right) + \frac{1}{2}(u^2 + v^2) \tag{3}$$

where ε is the specific energy, ρ is the density, u, and v are the velocities per unit mass in the x and y directions, respectively.

3.2 | Geometry and meshing

The parametric study included different diaphragm positions and pressure ratios. Therefore, to implement all the boundary conditions for each diaphragm position, three primary geometries have been obtained first in the Design Modeller (Figure 4).

Meshing the flow domain was done using the uniform quadrilateral method, as shown in Figure 5. The two longitudinal edges of both the driver and driven sections were divided equally; the division length equalled 1 mm. Conducting a mesh dependence study was done by having the pressure distribution at the rapture time while increasing the number of elements. The independence of the mesh element number was achieved when using 300,000 elements with 306051 nodes. Previous studies only refined the meshing at the diaphragm location to shorten the computational time. However, in this study, the refinement took place within all the edges of the shock tube geometry. Although the refinement of the entire geometry increases the computational time, the results accuracy was sufficiently acceptable.

Although the mesh dependence study is a standard method in finding the best element size for the model, it is sometimes considered a time-consuming process. Orthogonal quality, ortho skew and aspect ratio are the three primary parameters in the fluent mesh statistics, indicating the mesh quality. Those values are usually compared with a given acceptable range mentioned in DeSalvo and Swanson[32] to examine the solution convergence's
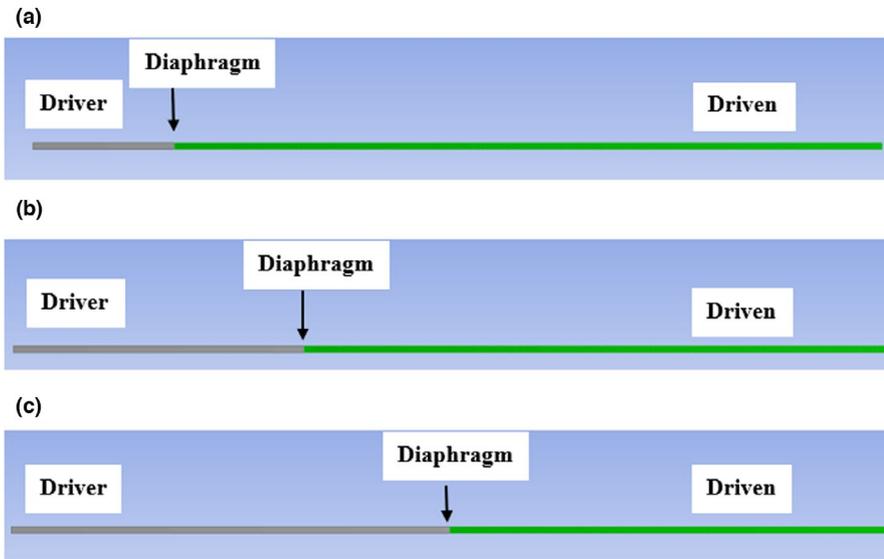
(a)

(b)

(c)

FIGURE 4 The geometry of the shock tube with different diaphragm positions; (A) diaphragm at 1m, (B) diaphragm at 2m and (C) diaphragm at 3m
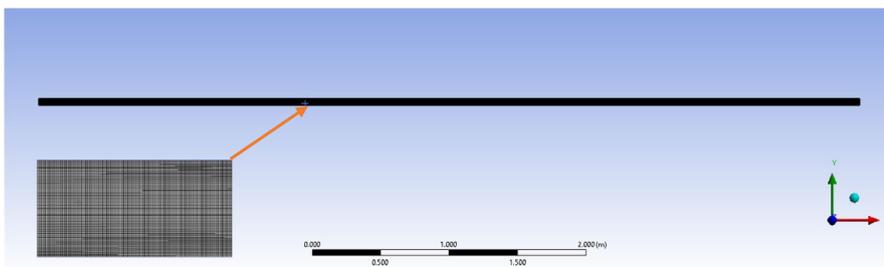

FIGURE 5 Meshing

TABLE 1 Mesh quality parameter

Mesh quality indicator	Value	Acceptable range
Minimum orthogonal quality	9.99996e−01	Above 0.01
Maximum ortho skew	3.76414e−06	Below 0.95
Maximum aspect ratio	2.79720e+00	Below 500

mesh quality range and time. Table 1 below shows the quality parameters assigned to the study mesh.

3.3 | Boundary conditions

In order to obtain a wave reflection from the shock tube-ends, the driver (high pressure) and driven (low pressure) section ends were closed. As a result, solid wall boundary was assigned to the edges of the 2D shock tube, and no fluid penetration occurred. The total length of the shock tube was 6 m, and the diaphragm was made by splitting the tube shape with a 2D edge. Diaphragm pressure was set to zero to eliminate its added pressure value to the pressure ratio between driven and driver sections. Since no heater was attached to the driver section, its initial temperature was 300°K (T_4). In contrast, as the driven section

TABLE 2 Initial boundary conditions of the numerical study

Boundary conditions	Working fluid			
	Ar (10%) + He (90%)		Air	
	P_4 (bar)	T_4 (kPa)	P_1 (kPa)	T_1 (K)
Case 1	6	300	1	423.15
Case 2	7	300	1	423.15
Case 3	8	300	1	423.15
Case 4	9	300	1	423.15
Case 5	10	300	1	423.15

was connected to heater coils, its initial temperature was chosen to be 423°K (T_1) in this study. All the initial condition values of the CFD simulation can be shown below in Table 2.

A density-based explicit solver was used to discretize the governing equation of the flow in time and space. To obtain an accurate and a stable solution, the conserved governing equation followed a double-precision second-order upwind scheme was used.[25] For the explicit time-dependent solution, the size of the time step was set to 1e-5 s, which provided convergence after ten iterations. The solution time interval duration was determined by the time step size (10e-5) and the number of time steps (2000).

4 | RESULTS AND DISCUSSION

The experiments were conducted for five pressure ratios with one diaphragm position (3m), while the simulation included all the suggested diaphragm positions for the five diaphragm pressure ratios. The same gas mixture (10% Ar and 90% He) was considered a working fluid for the experiment and numerical model. The shock tube performance was obtained based on the incident and reflected wave Mach number and the reflected wave temperature.

4.1 | Experimental results

As mentioned in the experimental set-up section, the velocity of the shock wave was measured by knowing the travel time of the shock wave between the two pressure sensors fitted in the driven section. Figure 6 illustrates the pressure readings of the two sensors versus time. The incident velocity could be easily obtained when the time difference between the two pressure peaks is known.

The experiment was repeated for the five pressure ratios, and five different shock wave velocities were recorded. The incident Mach number (M_i) associated with each wave velocity was obtained, as shown in Figure 10 below.

4.2 | Numerical results

When the diaphragm raptured at $t = 0$, the driver and driven pressures started changing from their initial values. Then, the driver pressure decreased in response to expansion wave formation. In contrast, the driven section pressure increased due to the developed compression wave propagation and diffusion. Eventually, the working fluid pressure across the tube reached a relaxing stage with an intermediate value. The pressure profile over the shock tube length was almost the same at the first time

increment of the transient study (0.1 ms), as shown in Figure 7.

The reflected wave (Mach number and temperature) properties present key performance indicators between several diaphragm position models. Since the ST was described as a 1-D problem, the pressure–temperature distribution only changed in the direction parallel to the flow with almost zero gradients perpendicular to the flow, Figure 8.

Figure 8A showed the pressure distribution at the first step (0.1 ms) after the rapture when the compression wave travelled along the driven section. The flow discontinuity and the contact surface are shown in Figure 8B when the wave is reflected from the driven end-wall. As expected, the wave reflected with high pressure and temperature, exceeding the value of P_4. However, the time required for the wave to reach the driven and driver end-wall is directly proportional to the distance between the diaphragm and the end-walls. In other words, in this study, a 1m change in the diaphragm position has resulted in a 0.13 ms change in the wave reflection from the driver end-wall. The previous rule applies to the two reflected waves: expansion and compression. Therefore, in Figure 8B, the reflected expansion wave could not be detected in positions (1m and 2m) for the selected time (0.69 and 0.56 ms), as the expansion waves have already been reflected and reached a relaxed sonic condition.

4.3 | Validation

The validation of the numerical model was conducted by comparing its incident Mach number (M_i) values against those observed from the ST experiment. Only one diaphragm position was adopted in the comparison study (middle position) while including the pressure ratios ranging from 6 to 10.

As illustrated in Figure 9, the M_i values follow an increasing trend with increased pressure. However, the
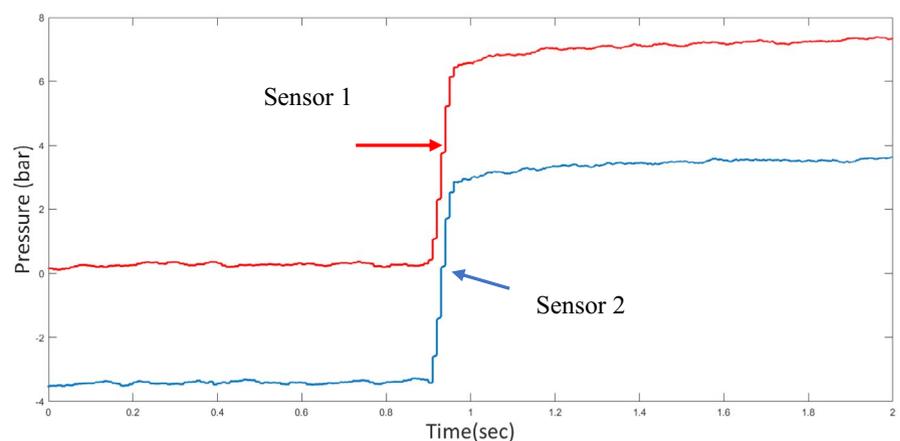

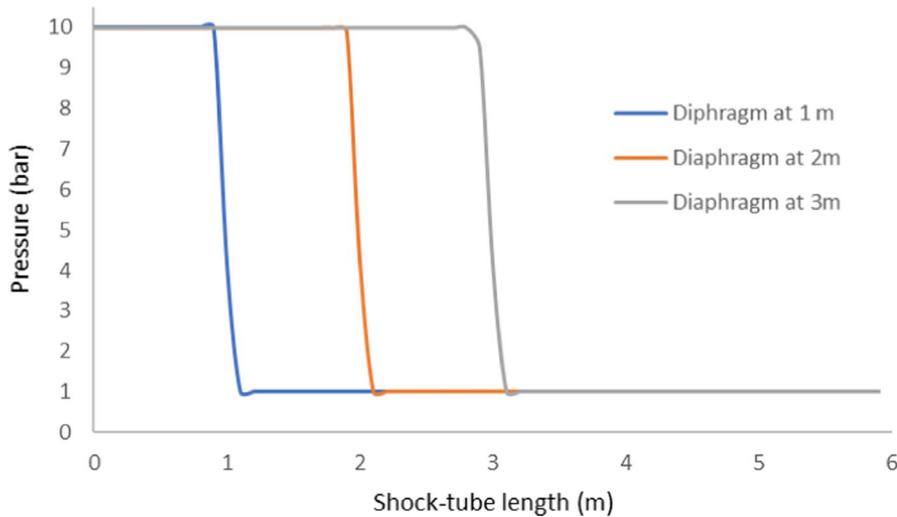**FIGURE 6** Sample results of the experiment at $P_4 = 8$ bar

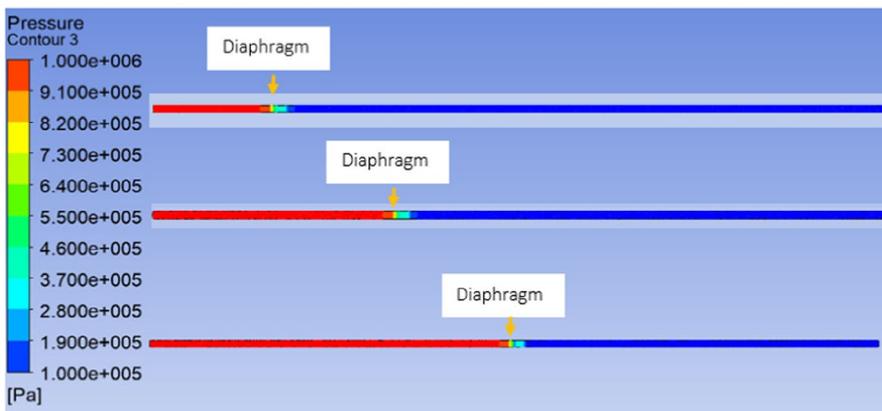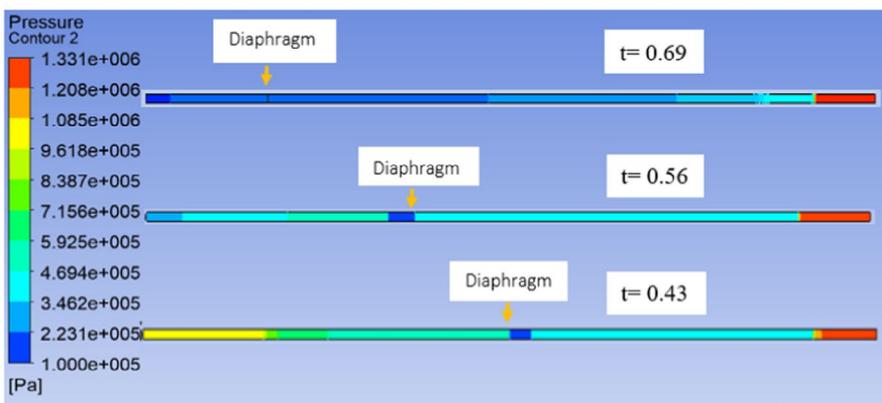**FIGURE 7** Pressure distribution at the rapture incident (0.0001 s)

FIGURE 8 Pressure contour (A) at the incident of rapture (B) after compression wave reflected from the driver section end-wall

numerical results are approximately 6% higher than the experimental ones at low-pressure values. This may be due to the viscous effect of the gas mixture at low pressure, which can be a source of non-idealizes factors of the ST.[33] This leads to shock tube attenuation phenomena, which implies that the shock wave amplitude decreases with distance from the diaphragm. Therefore, the incident shock attenuation is primarily due to boundary layer accumulation and non-ideal diaphragm rupture.[34,35] In contrast, a deviation of about 1% was obtained between 9 and 10 pressure ratios, indicating the reduction of the viscous losses.

4.4 | Parametric results

M_i dependency on diaphragm position and pressure ratios was combined in one graph, as shown in Figure 10.
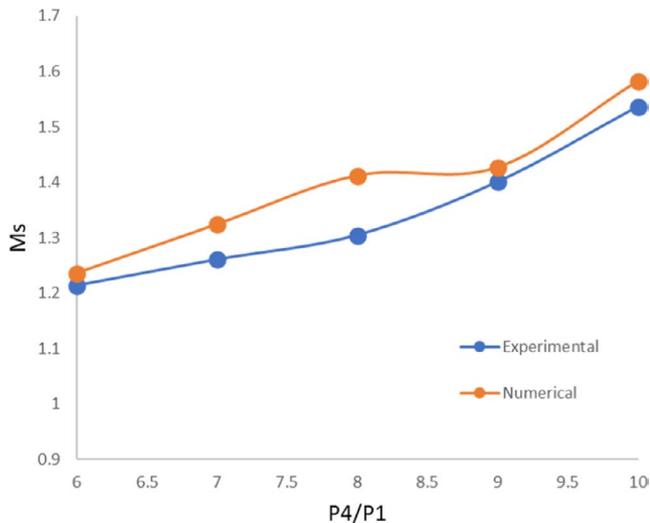
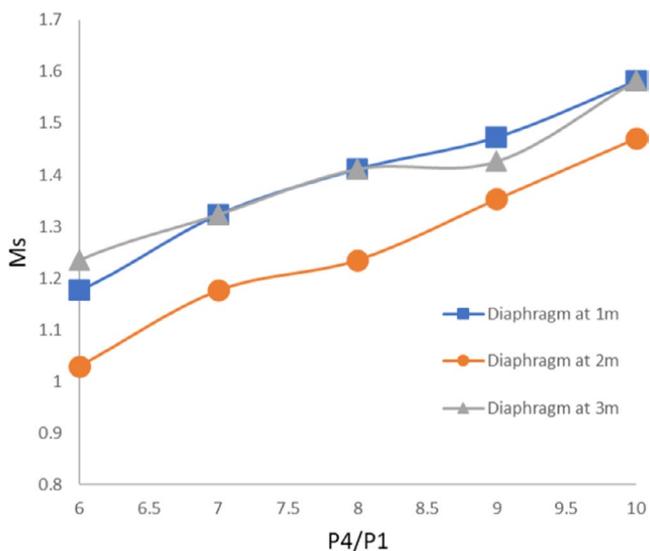**FIGURE 9** Diaphragm pressure ratio vs. incident Mach number (M_i)

FIGURE 10 Incident Mach number dependency on diaphragm location and pressure ratio

Figure 10 compares the effect of the pressure ratio on M_i value for the three diaphragm positions. As the diaphragm pressure ratio increases, the velocity of the shock wave and, hence its associated Mach number, rises significantly. However, when the diaphragm was located at 2m from the left end, the wave Mach number was about 20% lower than the Mach number obtained at other diaphragm positions: 2m and 3m. On the contrary, the two diaphragm locations, 1m and 3m, developed approximately the same Mach numbers for the tested pressure ratios except for 6 and 9 pressure ratios. In the pressure ratio 6 at the diaphragm Position no. 1, the Mach number was 5% higher than the Mach number provided by Position no. 3

for the same pressure value. It was clearly shown that the diaphragm Position no. 2 gave an overall reduction of 13% in Mach number compared with the other two positions.

The wave velocity increased significantly when the shock wave was reflected from the driven end-wall with high temperature and pressure.[36,37] Hence, the Mach number associated with the reflected wave (M_r M_r) was higher than the incident one. It is clearly shown in Figure 11 that M_r was almost independent of the diaphragm position except for pressure ratio 10 when the diaphragm position-3 model tended to have a higher value.

The temperature behind the reflected wave is also essential in finding the IDT of a fuel using the ST set-up. Figure 12 shows the pressure ratio effect on the reflected wave temperature (T_5) relative to the initial temperature of the driven section before the rapture (T_1). As the pressure ratio increased, the temperature behind the reflected shock wave increased for all the diaphragm positions. For example, for all the diaphragm position models, the temperature T_5 in pressure ratios (6–7) had the same values of about 850–900°K. However, at high-pressure ratios (10–8), the diaphragm Position no. 3 gave the highest T_5 values of about 1020°K, 975°K and 950°K compared with other positions. In addition, the T_5 temperature of the diaphragm Position no. 3 was almost 10°K higher than the T_5 diaphragm of Position 1, and 20K higher than T_5 of the diaphragm Position no. 2.

The usage of the ST as a facility for (IDT) investigations has been dominant for decades. More than 300 published studies with different test conditions for several types of fuels and many kinds of shock tube designs have findings related to chemical kinetics and particularly ignition delay.[34,38,39,40,41,42,43,44,45] This is due to that it is instantly (in microseconds) brings the reactive gas mixture to a well-defined temperature and pressure so that quick chemical reactions may be studied under zero-dimensional circumstances without affecting transport processes. When conducting ignition delay investigations, the shock tube was often calibrated by measuring the IDT of fuels and presenting it over the range of temperatures and pressures that had been determined. As stated by the Rankine–Hugoniot equations,[46] a given Mach number and shock velocity derive the pressure (P_5) and temperature (T_5) necessary. However, the diaphragm along the ST can be mounted in any position along the tube, affecting the finding of Mach number and thus the IDT. Therefore, diaphragm Position no. 2 was more suitable for finding the IDT of gaseous fuel than other positions, as it required a low Mach number. However, for the gaseous fuels,[39,41,42,45,47] the diaphragm location follows Position no. 2 (approximately the driven and driver section have the same length). In contrast, diaphragm position-1 and position-3 models were pretty ideal in finding the IDT of Diesel fuels, as they provided a high
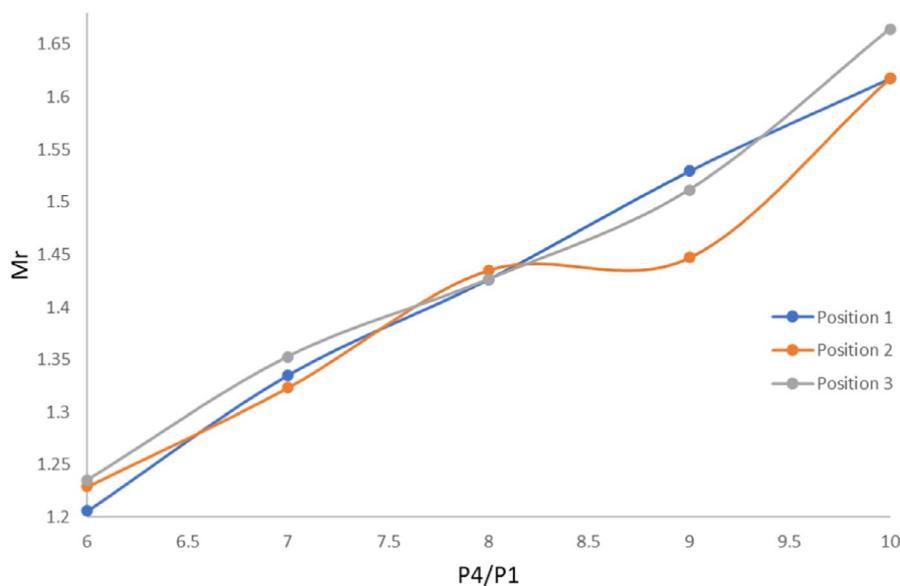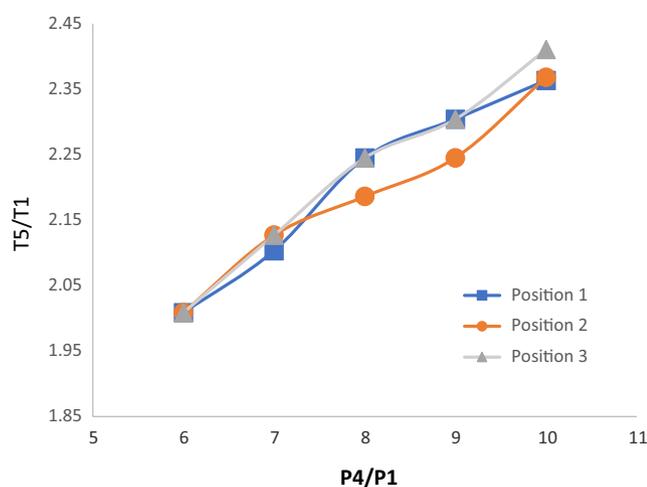
FIGURE 12 The change in reflected wave temperature with the diaphragm location and pressure ratio

Mach number and high reflected wave temperature values as in the references[48-55]

5 | CONCLUSIONS

This work presented an investigation of the parameters that affect a heated shock tube performance experimentally and numerically. The ST working fluid combined an Ar-He mixture in the driver section and air in the driven section. The ST set-up was operated under five pressure ratios while locating its diaphragm in the middle. Along with the experimental setup, a two-dimensional ST geometry was simulated using the transient inviscid model. The numerical parametric study introduced three different diaphragm positions and pressure ratios. The results

mainly depend on finding the Mach number correspondent to each condition (diaphragm pressure and location). The numerical model appeared to simulate the real case scenario of the ST when validating the model results with experiments. Based on the parametric study of the numerical model, one can state that:

1. The understudy experimental ST set-up can be simulated numerically using the 2D inviscid-transient CFD model with an acceptable error of less than 6% over the pressure ratio range.
2. When the diaphragm pressure ratio increased, the incident and reflected Mach numbers increase could be obtained for all three diaphragm position models.
3. Diaphragm position-2 model gave a low supersonic shock wave Mach number, and low reflected shock wave temperature values compared with the other two positions. In contrast, diaphragm Positions 1 and 3 almost produced the same high incident and reflected Mach numbers and the reflected shock wave temperature.
4. As the diaphragm was located near the driver end-wall, a high rapture pressure was generated, and hence, a high wave velocity can be obtained. On the contrary, the expansion wave (State 3) required less time to arrive at the driver end-wall and relaxed to sonic conditions. Therefore, diaphragm Position 3 (in the middle of the ST) provided a good compromise between staring gas pressure at the rapture and the expansion relaxation time effect.

NOMENCLATURE

ST	shock tube
ICE	internal combustion engine
IDT	ignition delay time
RCM	rapid compression machine
CVB	constant volume bomb
CFD	computational fluid dynamics
2D	two dimensions
MFC	mass flow controllers
u	velocity in x_direction per unit mass
v	velocity in y_direction per unit mass
P	pressure
T	temperature
ρ	density
M	Mach number

Subscripts

i	incident shock wave
r	reflected shock wave
1	initial condition in the driven section before rapture
2	incident Shock Wave condition at the driven section
3	the region behind expansion fan wave
4	initial condition in the driver section before rapture
5	reflected shock wave initial condition

ORCID

Samer F. Ahmed https://orcid.org/0000-0003-4235-4213

REFERENCES

1. Birch RS, Gerges SN, Vergara EF. Design of a pulse generator and shock tube for measuring hearing protector attenuation of high-amplitude impulsive noise. *Appl Acoust*. 2003;64(3):269-286. doi:10.1016/S0003-682X(02)00088-9
2. Gopalan J. Novel applications of micro-shock waves in biological sciences Novel applications of micro-shock waves in biological sciences, no. January 2002, 2014.
3. Jagadeesh G. Industrial applications of shock waves. *Proc Inst Mech Eng Part G J Aerosp Eng*. 2008;222(5):575-583. doi:10.1243/09544100JAERO306
4. Marty A, Daniel E, Massoni J, et al. Experimental and numerical investigations of a shock wave propagation through a bifurcation. *Shock Waves*. 2019;29(2):285-296.
5. Burden S, Tekawade A, Oehlschlaeger MA. Ignition delay times for jet and diesel fuels: constant volume spray and gas-phase shock tube measurements. *Fuel*. 2018;219:312-319. doi:10.1016/j.fuel.2018.01.113
6. Cooper SP, Mathieu O, Schoegl I, Petersen EL. High-pressure ignition delay time measurements of a four-component gasoline surrogate and its high-level blends with ethanol and methyl acetate. *Fuel*. 2020;275:118016. doi:10.1016/j.fuel.2020.118016
7. Davidson DF, Shao JK, Choudhary R, Mehl M, Obrecht N, Hanson RK. Ignition delay time measurements and

modeling for gasoline at very high pressures. *Proc Combust Inst*. 2019;37(4):4885-4892. doi:10.1016/j.proci.2018.08.032
8. Wang S, Mao Y, Raza M, Yu L, Lu X. Autoignition of diesel/oxygen/nitrogen mixture under elevated temperature in a heated shock tube. *Fuel*. 2019;254:115635. doi:10.1016/j.fuel.2019.115635
9. Abdellatif YM, Saker AT, Elbashir AM, Ahmed SF. Combustion and emissions of a gas-to-liquid (GTL) diesel engine utilizing optimized spiral-helical intake manifold designs. *J Energy Res Technol*. 2021;143:062308-1.
10. Ebrahemi AE, Bassiony MA, Syam TMI, Ahmed S. Investigating the effect of the air inlet temperature on the combustion characteristics of a spark ignition engine fueled by biogas. *Greenhouse Gases: Science and Technology*. 2020;10(4):771-782. doi:10.1002/ghg.1988
11. Bassiony MA, Sadiq AM, Gergawy MT, Ahmed SF, Ghani S. Investigating the effect of utilizing new induction manifold designs on the combustion characteristics and emissions of a DI diesel engine. *J Energy Res Technol*. 2018;140(12):122202-122217.
12. Elbashir AM, Saker AT, Ahmed SF. Effect of utilizing a novel intake manifold design on smoke emissions and particulate size distributions of a gas-to-liquid (GTL) diesel engine. *J Energy Resour Technol*. 2021;144:022301-1.
13. Sadeq AM, Bassiony MA, Elbashir AM, Ahmed SF, Khraisheh M. Combustion and emissions of a diesel engine utilizing novel intake manifold designs and running on alternative fuel. *Fuel*. 2019;255:115769.
14. Heywood JB. *Internal Combustion Engine Fundamentals By John B. Heywood*. McGraw-Hill Book Company; 1988.
15. Tranter RS, Giri BR. A diaphragmless shock tube for high temperature kinetic studies. *Rev Sci Instrum*. 2008;79(9):094103. doi:10.1063/1.2976671
16. Nagaraja SR, Prasad JK, Jagadeesh G. Theoretical – experimental study of shock wave-assisted metal forming process using a diaphragmless shock tube. *Proc Inst Mech Eng G J Aerosp Eng*. 2012;226(12):1534-1543. doi:10.1177/0954410011424808
17. Hargis JW, Cooper SP, Mathieu O, Petersen EL, Guo B. Ignition delay time measurements of heavy hydrocarbons in an aerosol shock tube. In *AIAA Scitech 2020 Forum*, Vol. 1 PartF, no. January; 2020. p. 1-10. doi:10.2514/6.2020-2144
18. Haylett DR, Davidson DF, Hanson RK. Ignition delay times of low-vapor-pressure fuels measured using an aerosol shock tube. *Combust Flame*. 2012;159(2):552-561. doi:10.1016/j.combustflame.2011.08.021
19. Haylett DR, Davidson DF, Hanson RK. Second-generation aerosol shock tube: an improved design. *Shock Waves*. 2012;22(6):483-493. doi:10.1007/s00193-012-0383-x
20. Haylett DR, Lappas PP, Davidson DF, Hanson RK. Application of an aerosol shock tube to the measurement of diesel ignition delay times. *Proc Combust Inst*. 2009;32(1):477-484. doi:10.1016/j.proci.2008.06.134
21. Visualization F. Aerosol shock tube designed for ignition delay time measurements of low-vapor-pressure fuels and auto-ignition flow-field visualization. *Energies*. 2020;13(3):683.
22. Luan Y, Olzmann M, Magagnato F. Simulation of a shock tube with a small exit nozzle. *J Therm Sci*. 2018;27(1):34-38. doi:10.1007/s11630-018-0981-8
23. Sod GA. A survey of several finite difference methods for systems of non-linear hyperbolic conservation laws. *J Comput Phys*. 1978;27(1):1-31. doi:10.1016/0021-9991(78)90023-2

24. Moradi FM, Fard M, Mani MR, Mottaghipour M. Experimental and numerical investigation of AUT shock tube. *Eur J Exp Biol*. 2012;2(5):1820-1826.

25. Jayakumar A, Damam A, Kumar NA. Shock tube performance studies with air and carbon dioxide using numerical simulation. *IJSER*. 2015;5(7):970-975.

26. Kim D, Kim J. Numerical method to simulate detonative combustion of hydrogen-air mixture in a containment. *Eng Appl Comput Fluid Mech*. 2019;13(1):938-953. doi:10.1080/19942060.2019.1660219

27. Ma Z, Du W, Wang X, Lv E, Dong Y. Shock tube studies on ignition delay and combustion characteristics of oxygenated fuels under high temperature. *Int J Energy Res*. 2020;44(13):10101-10111. doi:10.1002/er.5624

28. Ananthu JP, Asok Kumar N. Performance evaluation of shock tube with helium and carbon dioxide using numerical simulation. *J Phys Conf Ser*. 2019;1240(1):012138. doi:10.1088/1742-6596/1240/1/012138

29. Bradley JN, Emrich RJ. Shock waves in chemistry and physics. *Am J Phys*. 1963;31(3):224-225. doi:10.1119/1.1969408

30. Omega Engineering Inc. https://www.omega.com/en-us/pressure-measurement/pressure-transducers. Accessed September 29, 2021.

31. Al-Falahi A, Yusoff MZ, Shuaib NH, Yusaf T. Flow instability in shock tube due to shock wave-boundary layer-contact surface interactions, a numerical study. *Eur J Sci Res*. 2009;30(1):164-176. http://www.eurojournals.com/ejsr.htm. Accessed August 20, 2021.

32. DeSalvo GJ, Swanson JA. *ANSYS engineering analysis system user's manual*. Swanson Analysis Systems; 1985.

33. Flower G. Concepts of model verification and validation; n.d.

34. Nativel D, Cooper SP, Lipkowicz T, Fikri M, Petersen EL, Schulz C. Impact of shock-tube facility-dependent effects on incident- and reflected-shock conditions over a wide range of pressures and Mach numbers. *Combust Flame*. 2020;217:200-211. doi:10.1016/j.combustflame.2020.03.023

35. Petersen EL, Hanson RK. Nonideal effects behind reflected shock waves in a high-pressure shock tube. *Shock Waves*. 2001;10(6):405-420

36. Haselbacher A, Balachandar S, Kieffer SW. Open-ended shock tube flows: influence of pressure ratio and diaphragm position. *AIAA J*. 2007;45(8):1917-1929. doi:10.2514/1.23081

37. Lamnaouer M. Numerical modeling of the shock tube flow fields before and during ignition delay time experiments at practical and during ignition delay time experiments at practical conditions. PhD Thesis. 2010. https://stars.library.ucf.edu/etd/4208/. Accessed June 2, 2021.

38. Heng Y, Li G, Liang J, Zhang Z. Ignition characteristics of ethanol – hydrogen mixtures with different hydrogen contents at elevated initial temperatures. *Fuel*. 2020;281(1178):118742. doi:10.1016/j.fuel.2020.118742

39. Jiang X, Chen J, Huang W, Zhao H. Interpreting the effect of hydrogen addition on the auto-ignition of branched alkane : a case study of iso-butane/hydrogen/O 2/Ar mixtures. *Fuel*. 2020;284:119019. doi:10.1016/j.fuel.2020.119019

40. Merkel AC, Ciccarelli G. Diesel spray ignition behind a reflected shock wave. *Combust Flame*. 2020;217:237-247. doi:10.1016/j.combustflame.2020.04.004

41. Merkel AC, Ciccarelli G. Visualization of lean methane-air ignition behind a reflected shock wave. *Fuel*. 2020;271:117617. doi:10.1016/j.fuel.2020.117617

42. Saxena S, Kahandawala MSP, Sidhu SS. A shock tube study of ignition delay in the combustion of ethylene. *Combust Flame*. 2011;158(6):1019-1031. doi:10.1016/j.combustflame.2010.10.011

43. Sundararaj AJ, Pillai BC, Subash AN, Haran AP, Kumar P. Investigation of ignition delay for low molecular weight hydrocarbon fuel by using shock tube in reflected shock mode. *J Geol Soc India*. 2019;93(2):218-222. 10.1007/s12594-019-1155-3

44. Wang BL, Olivier H, Gro H. Ignition of shock-heated H2-air-steam mixtures. *Combust Flame*. 2003;133:93-106. doi:10.1016/S0010-2180(02)00552-7

45. Yang C, Wang W, Li Y, Cheng X. Quantitative study on chemical effects of actual/simulated recirculated exhaust gases on ignition delay times of n-heptane /ethanol fuel blends at elevated temperature. *Fuel*. 2020;263:116327. doi:10.1016/j.fuel.2019.116327

46. ELPERIN, G. B. D. O. I. T. (2001). *Handbook of Shock Waves*, Vol. 1. A Harcourt Science and Technology Company; 2001. p. 553-585. doi:10.1016/B978-0-12-086430-0.50000-2

47. Dinh L, Zhang Y, Huang Z. ScienceDirect shock tube study on ignition delay of multi-component syngas mixtures e effect of equivalence ratio. *Int J Hydrogen Energy*. 2014;39(11):6034-6043. doi:10.1016/j.ijhydene.2014.01.170

48. Abu-Elyazeed OSM. On the ignition delay of two types of Castor oil bio-diesel using shock tube experiments. *Fuel*. 2015;144:157-163. doi:10.1016/j.fuel.2014.12.041

49. Davidson DF, Haylett DR, Hanson RK. Development of an aerosol shock tube for kinetic studies of low-vapor-pressure fuels. *Combust Flame*. 2008;155(1-2):108-117. doi:10.1016/j.combustflame.2008.01.006

50. Hoang VN, Thi LD. ScienceDirect experimental study of the ignition delay of diesel/biodiesel blends using a shock tube. *Biosys Eng*. 2015;134:1-7. doi:10.1016/j.biosystemseng.2015.03.009

51. Merkel AC, Ciccarelli G. Diesel spray ignition behind a reflected shock wave. *Combust Flame*. 2020c;217:237-247. doi:10.1016/j.combustflame.2020.04.004

52. Qiu Y, Zhou W, Feng Y, et al. An experimental and modeling study of autoignition characteristics of butanol / diesel blends over wide temperature ranges. *Combust Flame*. 2020;217:175-187. doi:10.1016/j.combustflame.2020.03.031

53. Saleh HE, Selim MYE. Shock tube investigation of propane – air mixtures with a pilot diesel fuel or cotton methyl ester. *Fuel*. 2010;89(2):494-500. doi:10.1016/j.fuel.2009.09.010

54. Tsuboi T, Hozumi T, Hayata K, Ishii K. Study of diesel spray combustion in air containing burnt gas using. *Combust Sci Technol*. 2005;177:513-537.

55. Justin Sundararaj A, Guna KR, William M. Experimental investigation of the effect of temperature on ignition of modified kerosene. *Int J Engine Res*. 2022;23(3):460-468. doi:10.1177/1468087420988191